The effect of mixed La-Y doping on water resistance of phosphate glass

LI, Ao, HU, Yanhong, LIU, Zhaogang, ZHANG, Xiaowei, DENG, Wei, WANG, Hongyuan, LI, Mei and WANG, Mitang

The effect of mixed La-Y doping on water resistance of phosphate glass

Ao Li [a, b], Yanhong Hu [b, c], Zhaogang Liu [b, c], Xiaowei Zhang [a, b, c], Wei Deng [d], Hongyuan Wang [e], Mei Li [a, b, c *], Mitang Wang [a, b, c *]

([a] School of Materials Science and Engineering, University of Shanghai for Science and Technology, Shanghai 200093, China;

[b] School of Material and Metallurgy, Inner Mongolia University of Science and Technology, Baotou 014010, China;

[c] Key Laboratory of Green Extraction & Efficient Utilization of Light Rare-Earth Resources, Ministry of Education, Baotou 014010, China;

[d] Materials and Engineering Research Institute, Sheffield Hallam University, Sheffield S1 1WB, UK;

[e] The Fourth Affiliated Hospital of Inner Mongolia Medical University, Baotou, 014032 China)

Abstract: In this work, the effect of mixed La-Y doping on the water resistance of xLa_2O_3-$(16-x)Y_2O_3$-$8Al_2O_3$-$10Na_2O$-$66P_2O_5$ (x=0, 4, 8, 12, 16 mol%) glasses was studied. The glass structure, glass transition temperature (T_g), dc conductivity (σ_{dc}) and water resistance of glass were respectively characterized by Fourier transform infrared spectroscopy (FTIR), differential scanning calorimeter (DSC), electrochemical workstation and water resistance test. The results show that with the gradual replacement of Y_2O_3 by La_2O_3, the value of $Q^{(2)}$ (Q^2 content as a percentage of the sum of Q^1 and Q^2 contents in

*Corresponding author. E-mail address: btwmt@126.com (Pro. M. T. Wang); btlm65@163.com (Pro. M. Li)

glass structure) and water resistance characterized by mass loss per unit surface area indicate strong “mixed rare earth effect”. It is obvious that the change of glass structure causes water resistance of glass to vary nonlinearly and exhibit a positive deviation from linearity. The results can provide some useful information for tailoring the chemical durability of glass by mixed rare earth doping.

Keywords: Phosphate glass; Water resistance; Mixed rare earth effect; Glass structure

1. Introduction

In recent years, phosphate glass has been widely used in many fields by virtue of its excellent properties. Phosphate glass has good biocompatibility and it can be completely degraded in vivo. The degradation rate of phosphate glass can vary by several orders of magnitude depending on the chemical composition, so that the degradation rate of glass can be adjusted in a wide range. In the field of biomedicine, phosphate glass can be used to prepare artificial bone, repair damaged nerves and act as a carrier for carrying radiopharmaceutical in cancer radiotherapy [1-3]; Phosphate glass has lower melting temperature and viscosity, higher coefficient of thermal expansion, and it has received much attention in the field of sealing materials [4, 5]; In the field of optical materials, phosphate glass has the advantages of high UV transmittance, low preparation temperature and optical transmission loss, it is used as host materials for preparing optical waveguide device, optical amplifier and solid state laser doped with neodymium elements [6]; Iron phosphate glass with high chemical durability and simple preparation process has been widely used in the field of solidification of nuclear waste [7]; The solid electrolyte prepared by phosphate glass has the performance of high conductivity, isotropy, no grain

boundary and good processability [8].

Functional phosphate glasses put forward extremely high demand for chemical durability. For example, the therapeutic effect of phosphate bioglass is achieved by controlling the degradation rate of glass as well as the specie and rate of ion release during the degradation process [9]; Phosphate laser glass will be eroded by water molecules during processing, transportation and service stages. The corrosion of glass surface by water molecules not only leads to subcritical crack growth, the OH^- produced in the process of corrosion will also reduce the luminous performance of phosphate laser glass [10-12]; The extremely high water resistance is required for phosphate glass used to nuclear waste immobilization, which ensures that the solidified body's unexpected contact with groundwater will not lead to a large number of radioactive elements release [13]. It is not difficult to find that the chemical durability of phosphate glass directly affects the application effect and service life of the material in different fields. Therefore, it is very necessary to study the chemical durability of phosphate glasses.

At present, there are many researches on the chemical durability of phosphate glasses and many control methods of chemical durability have been developed. However, it is still a question how to control the chemical durability of glass without significant fluctuation of other properties. When it comes to this issue, we have to mention MME (mixed modifier effect). Mixed modifier effect means that in the glass system, the total content of network modifier remains constant, and one type of network modifier is gradually replaced by another, during the process of gradual replacement, some properties of glass will deviate from the linear additivity. Especially, properties related to ion migration, such as viscosity,

ion diffusion, electrical conductivity, dielectric loss, hardness and chemical durability have a large deviation from linearity [14, 15]. The chemical durability of the glass can be effectively controlled by the MME [16-18]. At present, most researches regarding MME in phosphate glasses focus on mixed alkali effect and mixed alkaline earth effect [18-20]. Introduction of rare earths into phosphate glass has great influence on many properties including chemical durability [21, 22]. However, little research has been carried out on controlling the chemical durability of glass by mixed rare earth doping. Further, during the practical application of phosphate glass, water is the most common corrosive medium. Therefore, the water resistance of mixed La_2O_3-Y_2O_3 doped phosphate glass was studied in this work, which could provide a new idea for regulating the chemical durability of phosphate glass.

2. Experimental

2.1. Glass synthesis

Glass was prepared by melting the mixture of La_2O_3 (99.5% Aladdin), Y_2O_3 (99.5% Aladdin), Al_2O_3 (McLean 99.8%), $NH_4H_2PO_4$ (McLean 99.5%) and Na_2CO_3 (McLean 99.5%). All the raw materials were required analytical reagent grade. The specific chemical composition of xLa_2O_3-$(16-x)Y_2O_3$-$8Al_2O_3$-$10Na_2O$-$66P_2O_5$ (x=0, 4, 8, 12, 16 mol%) glasses is shown in Table1. The raw materials required for melting 100g glass were uniformly mixed and ground, then placed in a corundum crucible. The mixture was hold at 300 °C for 90 min and then melted at 1300 °C for 2 h, finally the homogenized melt was poured into the preheated graphite mold. After molding, the glasses annealed for 2 h in the temperature range of 460−480 °C depending on the composition, and then cooled in the

furnace.

Table 1 The chemical composition of samples (mol%)

Sample	Y_2O_3	La_2O_3	P_2O_5	Al_2O_3	Na_2O
X=0	16	0	66	8	10
X=4	12	4	66	8	10
X=8	8	8	66	8	10
X=12	4	12	66	8	10
X=16	0	16	66	8	10

2.2. Water resistance

The examined samples were cut into 20×20×4 mm pieces, sanded with 600, 800, 1000, 1200 and 1500 mesh sandpapers successively and polished by polishing powder until the surface was smooth without scratches, then accurately measured the surface area of glass pieces. Glass pieces were washed with anhydrous ethanol in ultrasonic oscillator for 15 minutes, then rinsed with deionized water and dried for use. The prepared glass pieces were placed in the PTFE bottle containing 50 ml deionized water. After 30 days of water resistance test at room temperature, the mass loss per unit surface area was calculated based on the mass loss in the aqueous solution and the surface area of the glass. The relative error in these measurements was about ±0.1 g/m^2.

2.3 Dc conductivity

Dc conductivity was measured by electrochemical workstation (Zahner IM6e). Glass sample is 10mm in diameter, which was drilled from 1 mm thick sheet. The surface of the glass was sanded to ensure that both the upper and lower surface were parallel, and then accurately measured the diameter and thickness, so as to calculate the dc conductivity. In

order to get the silver electrode, glass coated with conductive silver paste was sintered at 195 ℃ for 2 h. The measurement frequency range of glass conductivity was 20 mHz−1 MHz, and the measurement was taken every 50 K from 503 K to 653 K. The error of ionic conductivity is about 5% from the experiments and calculation.

2.4 Density, molar volume and oxygen density

According to Archimedes' principle, the density of glass was measured by the electronic densitometer (GH-128E) at room temperature, and the immersion liquid was distilled water. Each sample was measured three times, and the glass density was taken as an average of three measurements. The estimated error limits are ±0.01 g/cm^3. The relationship between molar volume (V_m), density (ρ) and relative molecular mass (M) of glass is as follows:

$$V_m = M / \rho$$

Oxygen density was calculated by dividing the mass of oxygen atoms in one mole of glass (m_o) by the molar volume of the glass.

$$m_O = M_O \times (3X_{Y_2O_3} + 3X_{La_2O_3} + 5X_{P_2O_5} + 3X_{Al_2O_3} + X_{Na_2O})$$

where, M_O is the atomic weight of oxygen, X is the mole fraction of each component in glass.

2.5 Glass transition temperature

DSC curve of glass was determined by differential scanning calorimeter (Netzsch STA 449C). Glass transition temperature can be obtained from DSC curve by tangent method, and the accuracy of T_g is ±1 °C. Glasses were broken, ground, and sifted through 100 mesh to prepare samples for testing. 15 mg powdered glass was tested. The test

temperature varied from room temperature to 1000 ℃ with a heating rate of 10 ℃/min. During the process of testing, nitrogen was used as protective gas and α-Al_2O_3 was used as standard reference material.

2.6 Fourier transform infrared spectroscopy

Ground glass powder and KBr powder were mixed and grinded in an agate mortar with a mass ratio of 1:100. Then the mixture was under the press of 20 MPa provided by the tablet press for 1−2 min to obtain translucent discs for testing. In this experiment, the infrared absorption spectra of the glasses were recorded by Fourier transforminfrared spectrometer (Perkin Elmer) in the range of 400−4000 cm^{-1} with the resolution of 4 cm^{-1} at room temperature.

3. Results and discussion

3.1 Effect of mixed La_2O_3-Y_2O_3 doping on water resistance

The water resistance of glass is characterized by the mass loss per unit surface area, and the result is presented in Fig. 1. It can be seen that with the gradual replacement of Y_2O_3 by La_2O_3, the mass loss per unit surface area of glass increases firstly and then decreases, varies nonlinearly and exhibits a positive deviation from linearity. It reaches maximum when the molar ratio of $[La_2O_3]/([La_2O_3]+[Y_2O_3])$ is 0.5. The experimental data indicates that mixed rare earth doping reduces the water resistance of the studied glass.

Hydrolytic process of phosphate glass can be generally divided into two stages. In the first stage, when the phosphate glass contacts with water, water molecules will permeate into the interior of glass, and then sodium ions in the surface layer of glass exchanges with H^+ and H_3O^+ from aqueous solution, finally a hydrated layer forms on the surface. In the

second stage, hydrated layer extends into the interior of glass, and the extending rate depends on the breaking rate of glass network in the hydrated layer. In phosphate glass, the destruction of the glass network is mainly due to the attack of H_2O and H^+ on P−O−P bond between the [PO_4] units in the hydration layer, which will cause chain-like structures in different lengths consisting of Q^1 and Q^2 units to break away from the glass network and enter the water solution (Phosphorus-oxygen tetrahedrons are usually classified by Q^i, "i" represents the number of bridging oxygen in [PO_4] unit). When the glass is hydrolyzed at a constant rate, the expansion rate of the hydration layer reaches a dynamic balance with the breaking rate of the P−O−P bond [23].

There are many factors affecting the hydrolysis of phosphate glass. In the research on the stage of water molecules diffusing and ion exchanging, it was found that mixed alkali effect can effectively reduce the rate of water molecules diffusing and ion exchanging in the hydration layer, and thereby obtain the effect of inhibiting the glass hydrolysis. It indicates that the difficulty degree of ion migration can significantly affect the water resistance of glass [24, 25]. In the hydrolysis process of glass network, compared with M−O−P bonds the P−O−P bonds are vulnerable to attack by water molecules, therefore cross-linked network structure formed by Q^3 units has the worst water resistance. It is generally recognized that, when the content of Q^1 is increased, the corresponding content of Q^2 will decrease, which leads to a decrease in the average chain length of chain-like structures. The longer the average length of chain-like structure, the more vulnerable it is to the attack by water molecules [26, 27]. In the glass networks, the field strength of the modifier ion affects the topology of the network forming atoms, thus affecting the

dissolution kinetics. The rigidity of the glass network can be enhanced by changing the network modifier. The more rigid glass structure will give the glass network greater chemical durability [28]. Therefore, in order to further explore the reason why the mass loss per unit surface area of glass positively deviates from linearity, ionic migration characteristics, changes in structural units and the effect of changes in network modification on structure should be studied during the process of gradual replacementof Y_2O_3 by La_2O_3.

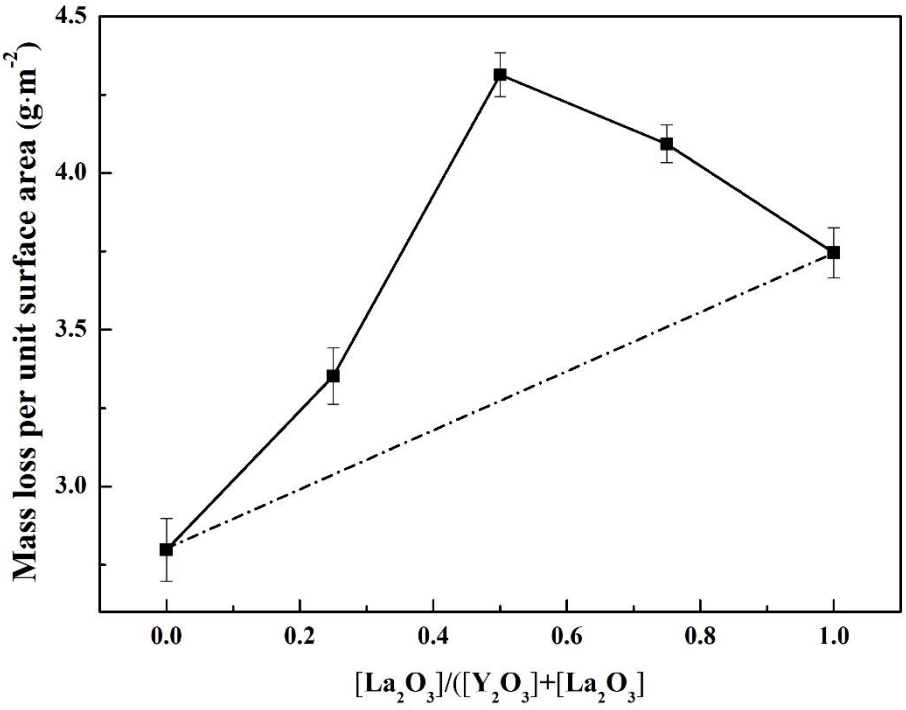

Fig. 1. Mass loss per unit surface area of xLa_2O_3-$(16-x)Y_2O_3$-$8Al_2O_3$-$10Na_2O$-$66P_2O_5$ glasses

3.2 Effect of mixed La_2O_3-Y_2O_3 doping on the ion migration

Although the research on MME has made some progress and established a series of theoretical models to describe the process of ion migration in glass, such as strong and weak electrolyte models, diffusion controlled relaxation model, jump diffusion model and dynamic structure model. However, the mechanism of MME and ion diffusion in glass

have not been determined so far [29-31]. The dc conductivity of glass can be used to characterize the difficulty degree of ion migration in glass. Therefore, the dc conductivity of mixed La-Y doped phosphate glass was studied.

Fig. 2 shows the conductivity spectra of $16Y_2O_3$-$8Al_2O_3$-$10Na_2O$-$66P_2O_5$ glass at different temperature. In the low frequency region, the conductivity of glass is independent of frequency and does not change with the increase of frequency, which reflect the dc conductivity of the glass. When the frequency exceeds a characteristic frequency, the conductivity will increase with the increases of the frequency. In this frequency range, it is hard for ionic charge carriers and network atoms to overcome the percolation barrier, so most of them forward-backward hopping [32-35].

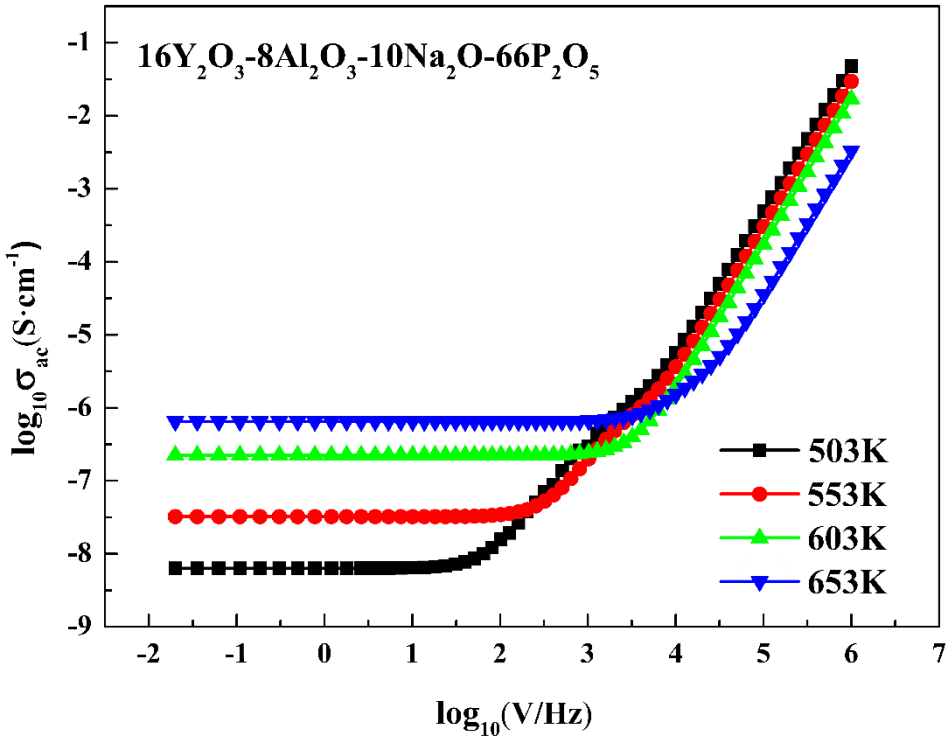

Fig. 2. Conductivity spectra of $16Y_2O_3$-$8Al_2O_3$-$10Na_2O$-$66P_2O_5$ glass at different temperature

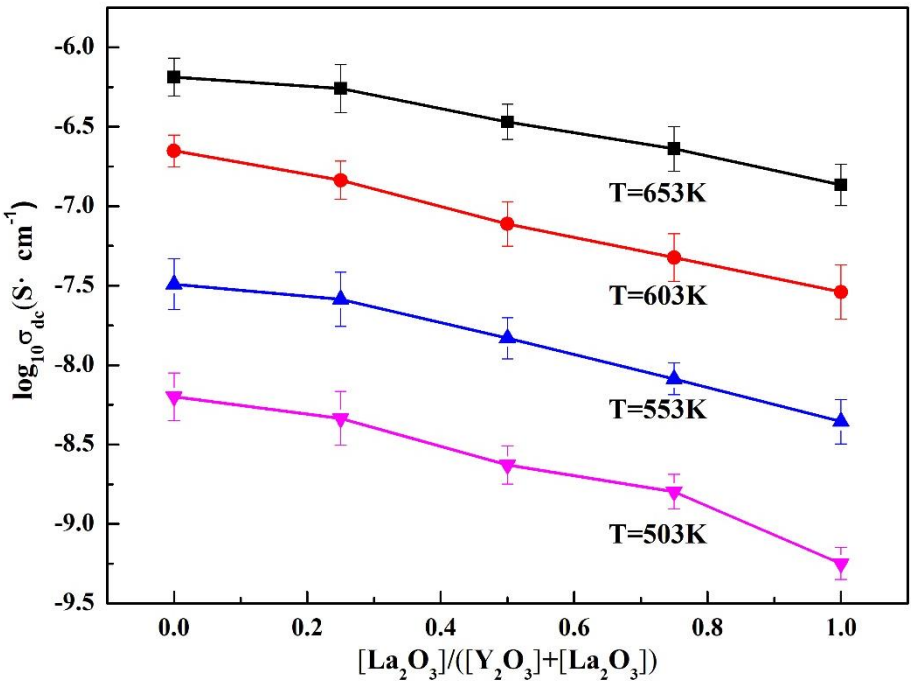

Fig. 3. The relationship between temperature and dc conductivity of xLa_2O_3-$(16-x)Y_2O_3$-$8Al_2O_3$-$10Na_2O$-$66P_2O_5$ glasses

The relationship between temperature and dc conductivity of xLa_2O_3-$(16-x)Y_2O_3$-8 Al_2O_3-$10Na_2O$-$66P_2O_5$ glasses is shown in Fig. 3. For the same glass sample, the higher the temperature is, the higher the dc conductivity of glass is. At the same temperature, with La_2O_3 gradually replaces Y_2O_3, the dc conductivity gradually decreases. It is obvious that Dc conductivity curves have a linear shape with the replacing content of La_2O_3. In order to research the effect of structural changes on dc conductivity, the density was measured and molar volume of glass was calculated. Fig. 4 shows density and molar volume, with the gradual replacement of Y_2O_3 by La_2O_3, density increases linearly and molar volume decreases linearly as the replacing content of La_2O_3 increase. Oxygen density is used to evaluate the compactness of the glass network. Oxygen density is shown in Fig. 5, with La_2O_3 gradually replaces Y_2O_3, the oxygen density gradually increases indicating that the

glass network become contracted [34, 35]. It is precisely the gradual contraction of the glass network that causes the molar volume decreases linearly. When substituting La_2O_3 for Y_2O_3, the atomic weight of La (138.91 g/mol) is higher than the atomic weight of Y (88.91 g/mol) and the glass network is gradually contracts during this substitution process, so the density of the glass increases linearly.

It suggests that the glass network gradually contracts and free volume gradually decreases with the increase of La_2O_3 doping amount. It is precisely the contraction of free volume that inhibits the migration of alkali ions [36, 37].

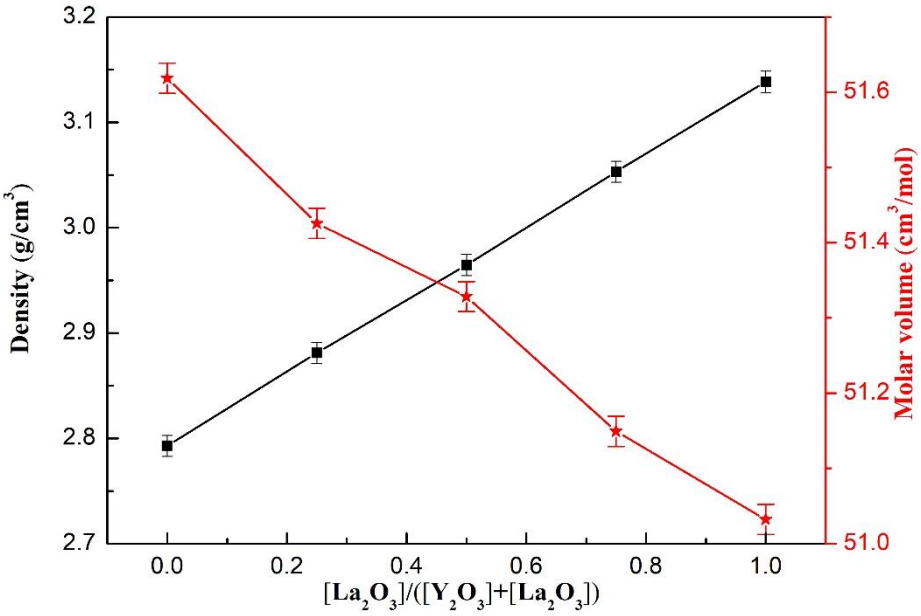

Fig. 4. The density and molar volume of xLa_2O_3-(16-x)Y_2O_3-8Al_2O_3-10Na_2O-66P_2O_5 glasses

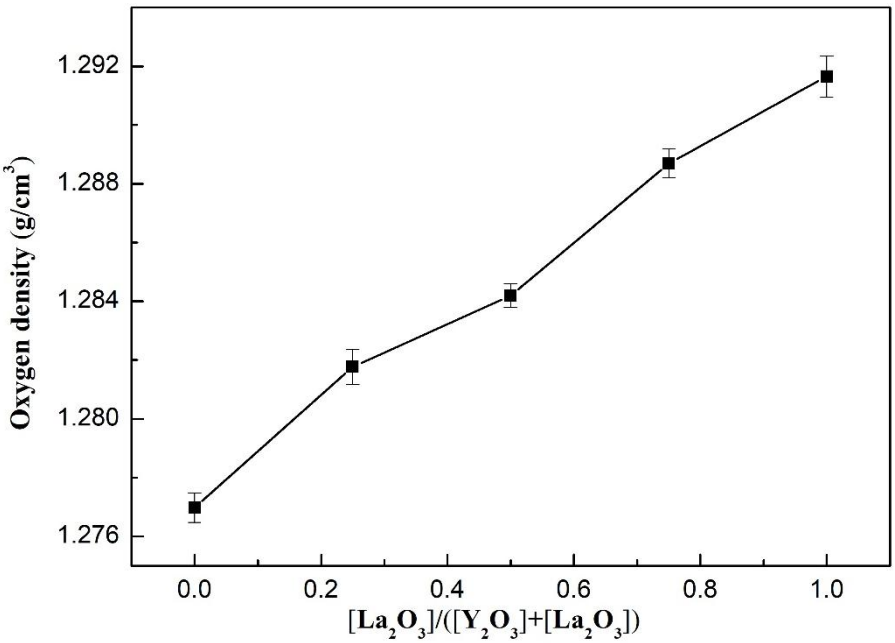

Fig. 5. The oxygen densityof xLa_2O_3-$(16-x)Y_2O_3$-$8Al_2O_3$-$10Na_2O$-$66P_2O_5$ glasses

From the conclusion of dc conductivity, with the gradual replacement of Y_2O_3 by La_2O_3, the migration of alkali ions in glass becomes more difficult and the dc conductivity gradually decreases. In this study, if the water resistance of glass is primarily related to the migration of alkali ions, the water resistance of glass will be enhanced with the increasing of the La_2O_3 content. In fact, the mass loss per unit surface area of glass varies nonlinearly and exhibits a positive deviation from linearity. It is clear that ion migration is not the dominant factor affecting the water resistance of glass in this experiment.

3.3 Effect of mixed La_2O_3-Y_2O_3 doping on glass structure

The glass transition temperature has a close relation with the glass structure [38]. Fig.6 shows DSC curves of xLa_2O_3-$(16-x)Y_2O_3$-$8Al_2O_3$-$10Na_2O$-$66P_2O_5$ glasses. The tangent method has been used to determine the T_g, the result is shown in Fig. 7. As La_2O_3 gradually replaces Y_2O_3, the T_g of glass decreases from 537 ℃ to 524 ℃ and has a linear

relation with the content of La_2O_3.

The field strength of Y^{3+} (3.70 $Å^{-2}$) is higher than that of La^{3+} (2.81 $Å^{-2}$). With the low field strength ions gradually replace the high field strength ions, the glass transition temperature decreases gradually. Generally, the higher the T_g is, the more rigid glass structure will be [39, 40]. In present research system, if only from the perspective of network modifier, with the replacing content of La_2O_3 increasing, water resistance of glass will decrease linearly. However, the fact that the water resistance of glass varies nonlinearly, it means that other factors, rather than network modifier mainly affect the water resistance of glass. Thereby, in order to research the effect of structural unit changes on water resistance of glass, FT-IR spectra of studied glasses were recorded and deconvoluted.

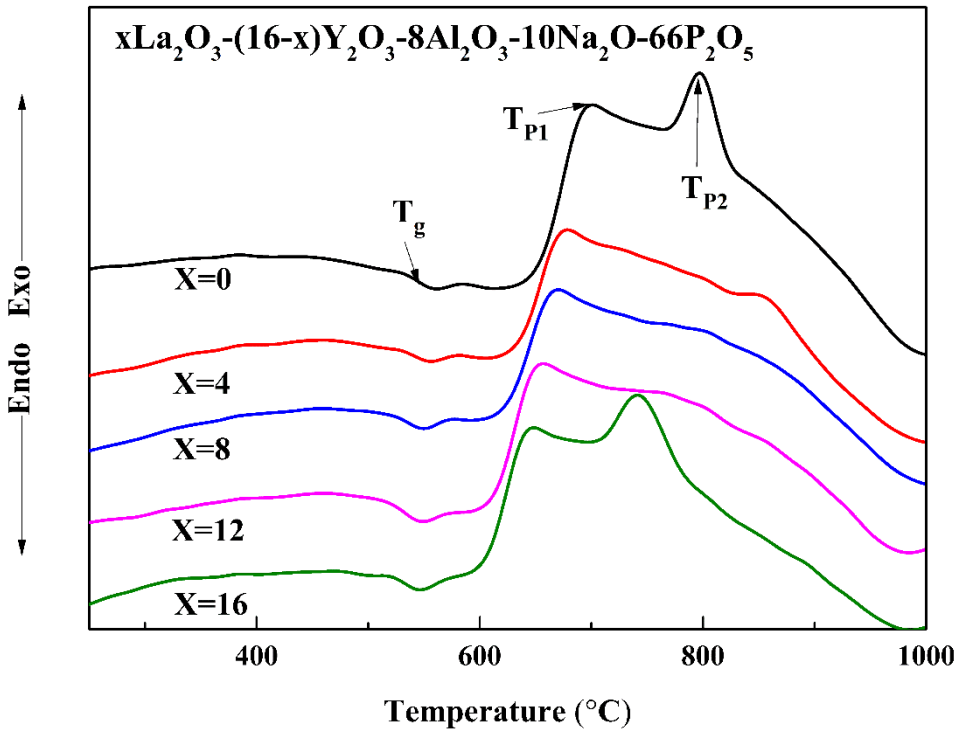

Fig. 6. DSC curves of xLa_2O_3-(16-x)Y_2O_3-8Al_2O_3-10Na_2O-66P_2O_5 glasses. T_g (glass transition temperature), T_{P1} (the first peak crystallization temperature), T_{P2} (the second peak crystallization temperature)

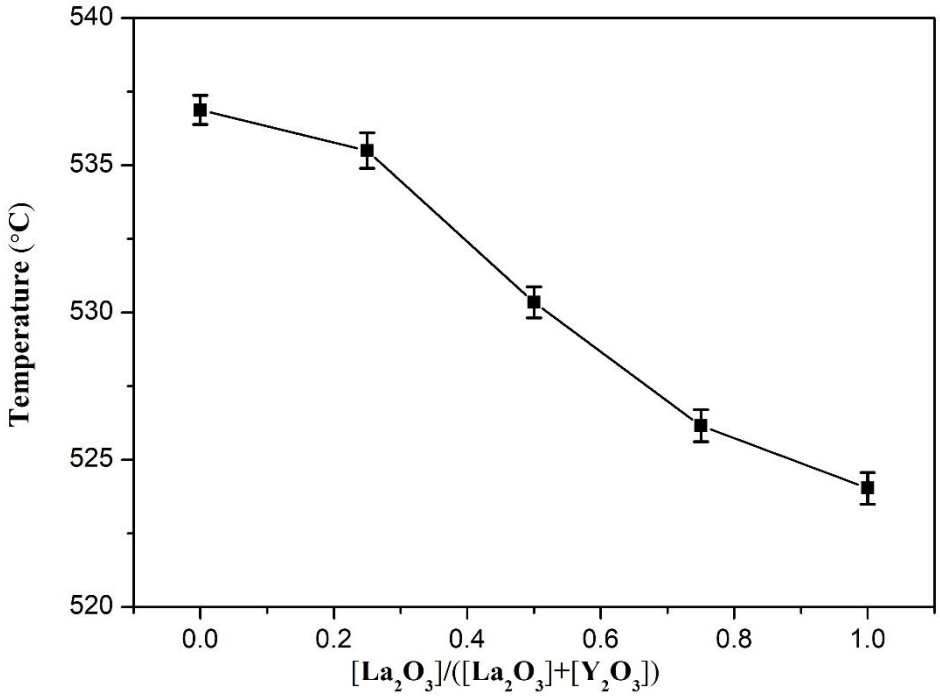

Fig. 7. T_g of xLa_2O_3-$(16-x)Y_2O_3$-$8Al_2O_3$-$10Na_2O$-$66P_2O_5$ glasses

Pure P_2O_5 glass is composed of $[PO_4]$ tetrahedrons. In each $[PO_4]$ tetrahedron there are three bridging oxygens connecting with adjacent tetrahedrons and another oxygen atom forming P=O with a phosphorus atom. Therefore the P_2O_5 glass has a three-dimensional layered network structure. In pure phosphate glass O/P = 2.5, and the cross-linked network is formed by Q^3 units. With the increasing of the doping content of metallic oxide, the number of non-bridging oxygen is increased, when 2.5<O/P<3, cross-linked network structure formed by Q^3 units is partially converted into chain-like structure which formed by Q^2 units; At O/P =3, metaphosphate glass is formed, and the glass network is entirely based on chain and ring structures. These chain and ring structures are connected by ionic bonds between metal cations and non-bridging oxygens; If the number of non-bridging oxygens continues increasing, when 3<O/P<3.5, part of Q^2 units will be converted into Q^1 units, which curtails the average chain length of chain-like structures formed by Q^2 units;

Pyrophosphate glass will be formed when O/P = 3.5, the glass network is mainly composed of phosphate dimers and each phosphate dimer consists of two Q^1 units linked by a bridging oxygen. When O/P>3.5, isolated Q^0 units appear in the glass structure, and its content increases as the number of non-bridged oxygen increases [41].

In present research system, the ratio of O/P is calculated to be 3.12. According to the structure theory of phosphate glass, there are almost no Q^3 units in glass structure which is mainly composed of Q^2 and Q^1 units. When the O/P>3, the mutual conversion of $2Q^1 \leftrightarrow Q^0+Q^2$ exists in the structural units of glass [42]. Due to the mutual conversion between structural units, a small amount of Q^0 units will be formed, and Q^0 is an isolated unit which does not affect the length of the chain-like structure. So in this paper, lays emphasis on the research of the changes of the relative contents of Q^2 and Q^1 units by infrared spectroscopy. FTIR spectra of xLa_2O_3-$(16-x)Y_2O_3$-$8Al_2O_3$-$10Na_2O$-$66P_2O_5$ (x=0, 4, 8, 12, 16 mol%) glasses are shown in Fig. 8. In order to quantify the changes of the glass structural units, FT-IR spectra are deconvoluted in the range of 400−1600cm^{-1}. For example, Fig. 9 shows deconvoluted FT-IR spectrum of $16La_2O_3$-$8Al_2O_3$-$10Na_2O$-$66P_2O_5$ glass.

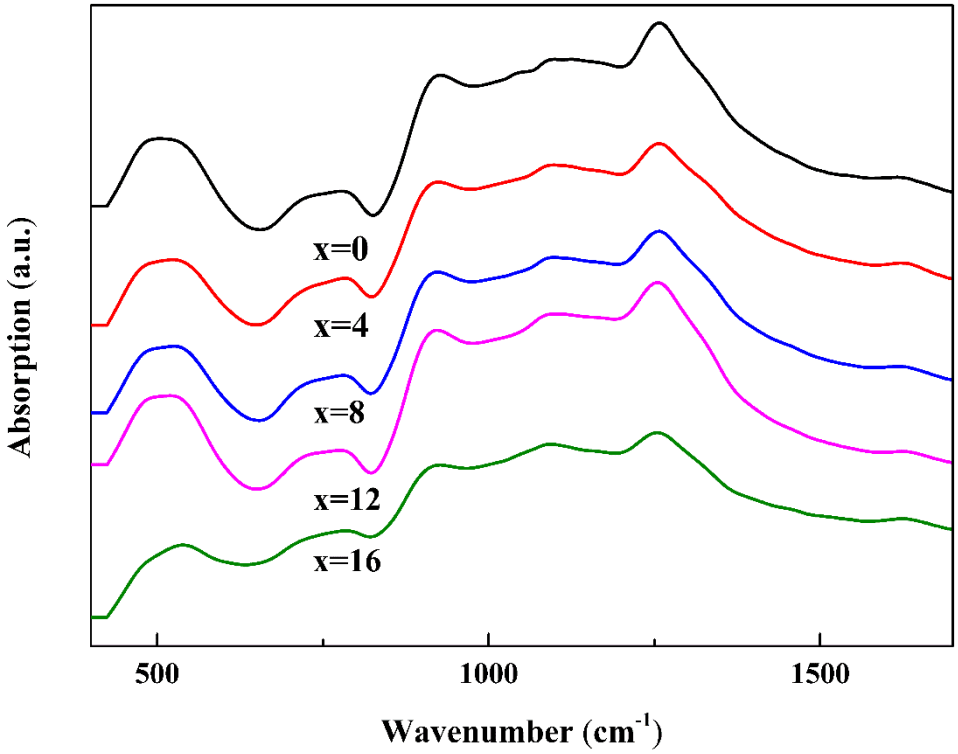

Fig. 8. FTIR spectra of xLa_2O_3-$(16-x)Y_2O_3$-$8Al_2O_3$-10 Na_2O-$66P_2O_5$ glasses

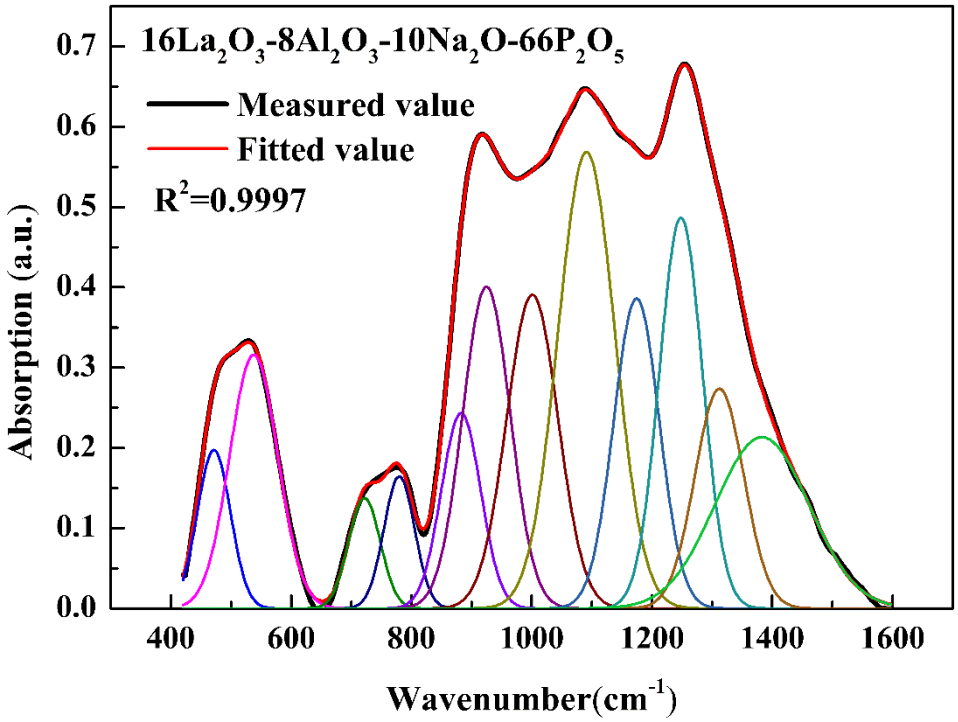

Fig. 9. Deconvoluted FT-IR spectrum of $16La_2O_3$-$8Al_2O_3$-$10Na_2O$-$66P_2O_5$ glass

The assignments of vibrational bands are shown in Table 2. The vibrational band in the range of 473 to 493 cm^{-1} can be attributed to harmonics of bending vibrations of

O−P−O and Al–O stretching vibrations [43-45]. The absorption band at 537−557 cm^{-1} is due to harmonics of bending vibrations of O=P−O linkages and Al−O stretching vibrations [43-46]. The vibrational band centered at 720−730 cm^{-1} is due to symmetric stretching vibrations of P−O−P in the Q^2 tetrahedron [47, 48]. The band appeared at 777−783 cm^{-1} is assigned to symmetric stretching vibrations of the bridging oxygen of P−O−P linkages of $(PO_3)^{2-}$ groups in Q^1 structural units [49, 50]. The band at 882−896 cm^{-1} is assigned to asymmetric stretching vibrations of P−O−P in Q^2 units linked with linear metaphosphate chain [45-47]. The peak around 925−933 cm^{-1} can be considered as asymmetric stretching vibrations of P–O–P in Q^2 units linked with large metaphosphate rings [46-48]. The band around 1001−1013 cm^{-1} is ascribed to symmetric stretching vibrations of $P-O^-$ bonds of $(PO_4)^{3-}$ groups in Q^0 units [45, 49, 50]. The assignment of the band between 1091 and 1113 cm^{-1} is associated to asymmetric stretching mode of chain-terminating Q^1 groups [45, 51]. The band at 1174−1191 cm^{-1} is related to symmetric stretching vibrations of non-bridging oxygens of O−P−O linkages of $(PO_2)^-$ groups in Q^2 units [45, 49]. The wavenumber of the band at 1248−1257 cm^{-1} is ascribed to asymmetric stretching vibrations of non-bridging oxygens of O−P−O linkages of $(PO_2)^-$ groups in Q^2 units [49, 50]. The band at 1300−1329 cm^{-1} is attributed to P=O asymmetric stretching mode of the phosphate tetrahedra [52]. The bands at 1372−1411 cm^{-1} is attributed to P=O stretching mode of the phosphate tetrahedra [52].

Table 2 Band assignment in the 400-1600 cm^{-1} range for studied phosphate glasses

Band frequency (cm^{-1})	Assignment
473−493	Harmonics of bending vibrations of O−P−O and Al–O stretching vibrations [43-45]
537−557	Harmonics of bending vibrations of O=P−O linkages and Al–O stretching vibrations [43-46]
720−730	Symmetric stretching vibrations of P−O−P in the Q^2 tetrahedra [47, 48]
777−783	Symmetric stretching vibrations of the bridging oxygens of P–O–P linkages of $(PO_3)^{2-}$ groups in Q^1 structural units [49, 50]
882−896	Asymmetric stretching vibrations of P−O−P in Q^2 units linked with linear metaphosphate chain [45-47]
925−933	Asymmetric stretching vibrations of P−O−P in Q^2 units linked with large metaphosphate rings [46-48]
1001−1013	Symmetric stretching vibrations of $P-O^-$ bonds of $(PO_4)^{3-}$ groups in Q^0 units [45, 49, 50]
1091−1113	Asymmetric stretching mode of chain-terminating Q^1 groups [45, 51]
1174−1191	Symmetric stretching vibrations of non-bridging oxygens of O−P−O linkages of $(PO_2)^-$ groups in Q^2 units [45, 49]
1248−1257	Asymmetric stretching vibrations of non-bridging oxygens of O−P−O linkages of $(PO_2)^-$ groups in Q^2 units [49, 50]
1300−1329	P=O asymmetric stretching mode of the phosphate tetrahedra [52]
1372−1411	P=O stretching mode of the phosphate tetrahedra [52]

Deconvolution parameters of FT-IR spectra for studied glasses are listed in Table 3. The $Q^{(2)}$ is used to quantify the changes of relative contents of Q^2 and Q^1 units, which represents the content of Q^2 structural units as a percentage of the total contents of Q^1 and Q^2 in glass. The calculation method of $Q^{(2)}$ and $Q^{(1)}$ are as follows [53]:

$$\begin{cases} Q^{(2)} = \dfrac{A_2}{A_1 + A_2} \times 100 \\ Q^{(1)} = 100 - Q^{(2)} \end{cases}$$

where A_2 is the sum of the absorption band areas related to the Q^2 structural units (bands center at 720−730 cm^{-1}, 882−896 cm^{-1}, 925−933 cm^{-1}, 1174−1191 cm^{-1} and 1248−1257 cm^{-1}), A_1 is the sum of the absorption band areas related to the Q^1 structural units (bands center at 777−783 cm^{-1} and 1091−1113 cm^{-1}).

Table 3 Deconvolution parameters of FT-IR spectra (C: band center (cm^{-1}), A: relative area (%))

X=0		X=4		X=8		X=12		X=16	
C	**A**	**C**	**A**	**C**	**A**	**C**	**A**	**C**	**A**
493	10.28	475	4.46	476	4.97	475	5.37	473	3.45
557	5.16	540	8.22	541	8.47	537	8.82	538	8.23
730	2.18	725	2.60	720	2.03	721	1.83	722	2.37
783	1.52	783	2.60	778	3.00	777	2.06	780	2.75
896	4.90	893	5.34	890	5.38	891	2.98	882	5.21
932	7.49	933	11.39	931	10.17	927	12.48	925	10.36
1009	14.86	1013	11.02	1005	10.50	1009	10.48	1001	10.95
1113	17.76	1100	15.97	1093	16.18	1097	16.49	1091	17.57
1191	8.29	1183	10.23	1176	10.69	1180	11.01	1174	9.55
1251	6.99	1250	7.43	1257	14.17	1251	10.85	1248	11.41
1300	10.11	1305	8.74	1329	7.39	1312	10.13	1312	7.26
1372	10.46	1374	12.00	1411	7.04	1399	7.50	1382	10.88

$Q^{(1)}$ and $Q^{(2)}$ are plotted as a function of $[La_2O_3]/([Y_2O_3]+[La_2O_3])$ in Fig. 10. It can be seen from the figure that as La_2O_3 gradually replaces Y_2O_3, the value of $Q^{(2)}$ increases firstly and then decreases, varies nonlinearly and has a positive deviation from linearity,

and $Q^{(2)}$ reaches maximum when the molar ratio of $[La_2O_3]/([La_2O_3]+[Y_2O_3])$ equals to 0.5. Correspondingly, the value of $Q^{(1)}$ decreases firstly and then increases, reaches minimum when the molar ratio of $[La_2O_3]/([La_2O_3]+[Y_2O_3])$ is 0.5. Accordingly, The non-linear variation of the relative contents of Q^2 and Q^1 units causes the average length of the chain-like structure increases firstly and then decreases, and has a positive deviation from the linear relationship, which consequently leads the mass loss per unit surface area of glass in the aqueous solution to increase firstly and then decrease, reach maximum when the molar ratio of $[La_2O_3]/([La_2O_3]+[Y_2O_3])$ equals to 0.5. The conclusions above indicate that the mixed rare earth doping reduces water resistance by affecting the structure of glass.

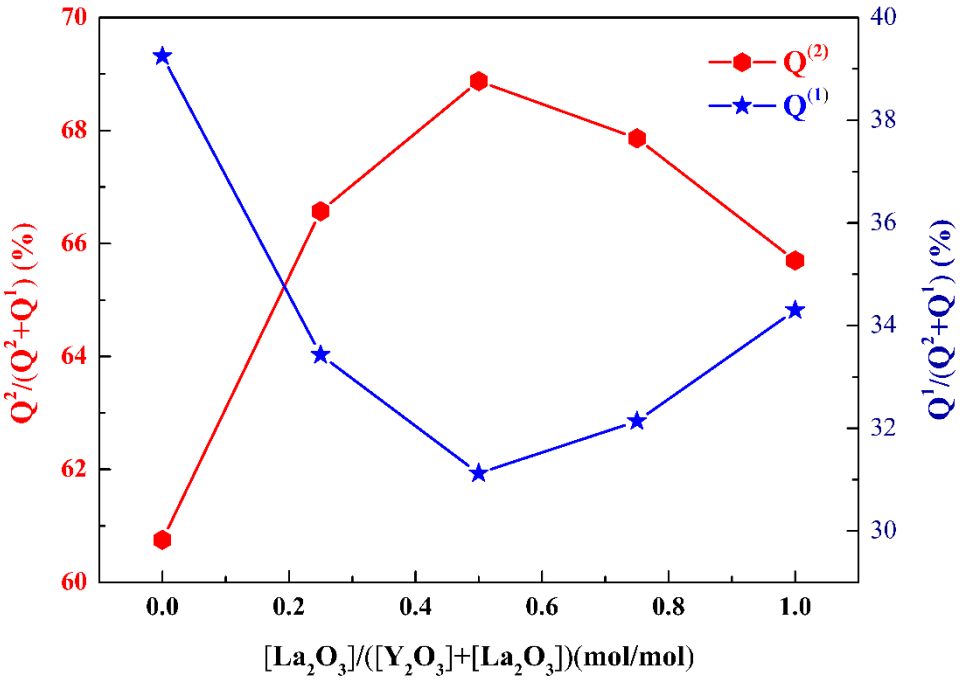

Fig. 10. $Q^{(1)}$ and $Q^{(2)}$ are plotted as a function of $[La_2O_3]/([Y_2O_3]+[La_2O_3])$

4. Conclusions

In xLa_2O_3-$(16-x)Y_2O_3$-$8Al_2O_3$-$10Na_2O$-$66P_2O_5$ (x=0, 4, 8, 12, 16 mol%) glasses, with the gradual replacement of Y_2O_3 by La_2O_3, the glass density gradually increases and the

molar volume gradually decreases. The decrease of molar volume causes that the free volume inside the glass gradually decreases, eventually leading to a decrease in the dc conductivity of the glass. In terms of glass structure, T_g decreases with an increase in the replacing content of La_2O_3. The mixed rare earth doping causes a nonlinear variation of $Q^{(2)}$ value in the glass structure. It is precisely the $Q^{(2)}$ value exhibits a nonlinear variation that causes the mass loss per unit surface area of the glass in the aqueous solution to vary nonlinearly and has a positive deviation from the linear relationship.The results show that the mixed rare earth doping weakens the water resistance of the studied glass. The results can provide some useful information for tailoring the chemical durability of glass by mixed rare earth doping.

Acknowledgements

This project is financially supported by National Natural Science Foundation of China (51974168, 51662033 and 51362019), Natural Science Foundation of the Inner Mongolia Autonomous Region (2016JQ05).

Declaration of Competing Interest

The authors declare that they have no known competing financial interests or personal relationships that could have appeared to influence the work reported in this paper.

References

[1] S. Thonglem, G. Rujijanagul, S. Eitssayeam, T. Tunkasiri, K. Pengpat, Fabrication of P_2O_5-CaO-Na_2O glasses doped with magnesium oxide for artificial bone applications, Ceram. Int. 39 (2013) 537−540.

[2] Y. Fu, J.K. Christie, Atomic structure and dissolution properties of yttrium containing phosphate glasses, Int J Appl Glass Sci. 8 (2017) 412−417.

[3] F. Baino, G. Novajra, V. Miguez-Pacheco, A.R. Boccaccini, C. Vitale-Brovarone, Bioactive glasses: Special applications outside the skeletal system, J. Non-Cryst. Solids 432 (2016) 15−30.

[4] T.Y. Wei, Y. Hu, L.G. Hwa, Structure and elastic properties of low-temperature sealing phosphate glasses, J. Non-Cryst. Solids 288 (2001) 140−147.

[5] J. Hong, D. Zhao, J. Gao, M. He, H. Li, G. He, Lead-free low-melting point sealing glass in SnO-CaO-P_2O_5 system, J. Non-Cryst. Solids 356 (2010) 1400−1403.

[6] J. Juarez-Batalla, A.N. Meza-Rocha, G. Muñoz H. I. Camarillo, U. Caldino, Luminescence properties of Tb^{3+}-doped zinc phosphate glasses for green laser application, Opt. Mater. 58 (2016) 406−411.

[7] A.S. Pinheiro, Z.M.D. Costa, M.J.V. Bell, V. Anjos, N.O. Dantas, S.T. Reis, Thermal characterization of iron phosphate glasses for nuclear waste disposal, Opt. Mater. 33 (2011) 1975−1979.

[8] S.S. Das, N.P. Singh, P.K. Srivastava, Ion conducting phosphate glassy materials, Prog. Cryst. Growth Charact. Mater. 55 (2009) 47−62.

[9] G. Novajra, J.Lousteau, D.Milanese, C. Vitale-Brovarone, Resorbable hollow phosphate glass fibres as controlled release systems for biomedical applications, Mater. Lett. 99 (2013) 125−127.

[10] M. Li, B. Wang, X. Wang, X. Yang, D. Chen, W. Chen, L. Hu. Water corrosion of commercial neodymium-doped phosphate high-peak-power laser glass, J. Non-Cryst. Solids 496 (2018) 34−41.

[11] J. Yu, Q. Jian, W. Yuan, B. Gu, F. Ji, W. Huang, Further damage induced by water in micro-indentations in phosphate laser glass, Appl. Surf. Sci. 292 (2014) 267−277.

[12] S. Xu, D. Fang, Z. Zhang, Z.Jiang. Effect of OH^- on upconversion luminescence of Er^{3+}-doped oxyhalide tellurite glasses, J. Solid State Chem. 178 (2005) 2159−2162.

[13] P.P. Poluektov, O.V. Schmidt, V.A. Kascheev, M.I. Ojovan, Modelling aqueous corrosion of nuclear waste phosphate glass, J. Nucl. Mater. 484 (2017) 357−366.

[14] C. Calahoo, J.W. Zwanziger, The mixed modifier effect in ionic conductivity and mechanical properties for xMgO-(50-x)CaO-50SiO_2 glasses, J. Non-Cryst. Solids 460 (2017) 6−18.

[15] A. Faivre, D. Viviani, J. Phalippou, Mixed alkali effect in Li and Na aluminophosphate glasses: influence of the cation environment, Solid State Ionics 176 (2005) 325−332.

[16] L. Hupa, S. Fagerlund, J. Massera, L. Björkvik, Dissolution behavior of the bioactive glass S53P4 when sodium is replaced by potassium, and calcium with magnesium or strontium, J. Non-Cryst. Solids 432 (2016) 41−46.

[17] A. Li, M. Wang, M. Li, Z. Liu, Y. Hu, X. Zhang,The effect of mixed alkali on structural changes and ionic migration Characteristics in zinc borate glasses, Mater. Chem. Phys. 217 (2018) 519−526.

[18] H.W. Guo, X.F. Wang, Y.X. Gong, D.N. Gao, Mixed alkali effect in xK_2O-(30-x) Na_2O-30P_2O_5-40ZnO glasses, J. Non-Cryst. Solids 356 (2010) 2109−2113

[19] X. Fang, C.S. Ray, D.E. Day, Glass transition and fragility of iron phosphate glasses: II. Effect of mixed-alkali, J. Non-Cryst. Solids 319 (2003) 314−321

[20] K. Griebenow, C.B. Bragatto, E.I. Kamitsos, L. Wondraczek, Mixed-modifier effect in alkaline

earth metaphosphate glasses, J. Non-Cryst. Solids 481 (2018) 447−456.

[21] Q. Shi, Y. Yue, Y. Qu, S. Liu, G.A. Khater, L. Zhang, J. Zhao, J. Kang, Structure and chemical durability of calcium iron phosphate glasses doped with La_2O_3 and CeO_2, J. Non-Cryst. Solids 516 (2019) 50–55.

[22] S.W. Yung, S.M. Hsu C.C. Chang, K.L. Hsu, T.S. Chin, H.I. Hsiang, Y.S. Lai, Thermal, chemical, optical properties and structure of Er^{3+}-doped and Er^{3+}/Yb^{3+} co-doped P_2O_5-Al_2O_3-ZnO glasses, J. Non-Cryst. Solids 357 (2011) 1328−1334.

[23] H. Gao, T. Tan, D. Wang, Dissolution mechanism and release kinetics of phosphate controlled release glasses in aqueous medium, J. Control Release 96 (2004) 29−36.

[24] B.M.J. Smets, M.G.W. Tholen, T.P.A. Lommen, The absence of a mixed-alkali effect in the leaching of corrosion-resistant glasses, J. Mater. Sci. 20 (1985) 1027−1032.

[25] M. F. Dilmore, D. E. Clark, L. L. Hench. Chemical Durability of Na_2O-K_2O-CaO-SiO_2 Glasses, J. Am. Ceram. Soc. 61(1978) 439−443

[26] F. Dohler, A. Mandlule, L.V. Wüllen, M. Friedrich, D.S. Brauer, ^{31}P NMR characterization of phosphate fragments during dissolution of calcium sodium phosphate glasses, J. Mater. Chem. B 3 (2015) 1125−1134.

[27] H. Masai, R. Shirai, T. Miyazaki, K. Yoshida, T. Fujiwara, Y. Tokuda, T. Yoko, Fabrication of $Sr_{0.5}Ba_{0.5}Nb_2O_6$ Nanocrystallite-Precipitated Transparent Phosphate Glass-Ceramics, J. Am. Ceram. Soc. 96 (2013) 3576−3583.

[28] T. Oey, K.F. Frederiksen, N. Mascaraque, R. Youngman, M. Balonis, M.M. Smedskjaer, M. Bauchy, G. Sant, The role of the network-modifier's field-strength in the chemical durability of aluminoborate glasses, J. Non-Cryst. Solids 505 (2019) 279 – 285.

[29] C.T. Moynihan, A.V. Lesikar, Weak-Electrolyte Models for the Mixed- Alkali Effect in Glass, J. Am. Ceram. Soc. 64 (1980) 40−46.

[30] M.M. Smedskjaer, S.J. Rzoska, M. Bockowski, J.C. Mauro, Mixed alkaline earth effect in the compressibility of aluminosilicate glasses, J Chem Phys. 140 (2014) 054511.

[31] J. Kjeldsen, M.M. Smedskjaer, J.C. Mauro, R.E. Youngman, L. Huang, Y. Yue. Mixed alkaline earth effect in sodium aluminosilicate glasses, J. Non-Cryst. Solids369 (2013) 61−68.

[32] B. Roling, C. Martiny, S. Murugavel, Ionic conduction in glass: new information on the interrelation between the "jonscher behavior" and the "nearly constant–loss behavior" from broadband conductivity spectra, Phys. Rev. Lett. 87 (2001) 085901.

[33] Y.C. Fredholm, N. Karpukhina, R.V. Law, R.G. Hill, Strontium containing bioactive glasses: Glass structure and physical properties, J. Non-Cryst. Solids 356 (2010) 2546–2551.

[34] M. Tylkowski, D.S. Brauer, Mixed alkali effects in Bioglass® 45S5, J. Non-Cryst. Solids376 (2013) 175 – 181.

[35] S. Ghosh, A. Ghosh, Ion dynamics and mixed mobile ion effect in fluoride glasses, J. Appl. Phys.

97 (2005) 123525.

[36] J. Swenson, L. Börjesson, Correlation between Free Volume and Ionic Conductivity in Fast Ion Conducting Glasses, Phys. Rev. Lett. 77 (1996) 3569−3572.

[37] D.L. Sidebottom, Influence of cation constriction on the ac conductivity dispersion in metaphosphate glasses, Phys. Rev. B 61 (2000) 14507−14516.

[38] F. Branda, F.A. Varlese, A. Costantini, G. Luciani, T_g and FTIR of (2.5-x)CaO·x/3M_2O_3·2SiO_2 (M=Y, La, In, Al, Ga) glasses, J. Non-Cryst. Solids 246 (1999) 27−33.

[39] J.E. Shelby, J.T.Kohli, Rare-earth aluminosillcate glasses, J. Am. Ceram. Soc. 73 (1990) 39−42.

[40] Y. Chenga, H. Xiao, W. Guo, Influence of rare-earth oxides on structure and crystallization properties of Bi_2O_3 – B_2O_3glass, Mater. Sci. Eng., A 480 (2008) 56−61.

[41] R.K. Brow, Review: the structure of simple phosphate glasses, J. Non-Cryst. Solids 263-264 (2000) 1−28.

[42] R.K. Brow, D.R. Tallant, S.T. Myers, C.C. Phifer, The short-range structure of zinc polyphosphate glass, J. Non-Cryst. Solids 191 (1995) 45−55.

[43] L. L. Velli, C. P. E. Varsamis, E. I. Kamitsos, Structural investigation of metaphosphate glasses, Phys. Chem. Glasses 46 (2005) 178−181.

[44] S.V. Stefanovsky, O.I. Stefanovskaya, S.E. Vinokurov, S.S. Danilov, B.F. Myasoedov, Phase Composition, Structure, and Hydrolytic Durability of Glasses in the Na_2O-Al_2O_3-(Fe_2O_3)-P_2O_5 System at Replacement of Al_2O_3 by Fe_2O_3, Radiochemistry 57 (2015) 348−355.

[45] A.A. Ahmed, A.A. Ali, Doaa A.R. Mahmoud, A.M. El-Fiqi, Study on the preparation and properties of silver-doped phosphate antibacterial glasses (Part I), Solid State Sci. 13 (2011) 981−992.

[46] Y.M. Moustafa, K. El-Egili, Infrared spectra of sodium phosphate glasses, J. Non-Cryst. Solids 240 (1998) 144−153.

[47] L.Y. Zhang, H. Li, L.L. Hu, Statistical structure analysis of GeO_2 modified Yb^{3+}: Phosphate glasses based on Raman and FTIR study, J. Alloys Compd. 698 (2017) 103−113.

[48] P. Stoch, A. Stoch, M. Ciecinska, I. Krakowiakc, M. Sitarza, Structure of phosphate and iron-phosphate glasses by DFT calculations and FTIR/Raman spectroscopy, J. Non-Cryst. Solids 450 (2016) 48−60.

[49] B. Johnson, B.K. Sudhakar, N.R.K. Chand, K. Rayapa Reddy, G. Srinivasa Rao, Structure-property relationships of Fe_2O_3 doped novel oxyfluorophosphate glasses, J. Non-Cryst. Solids 404 (2014) 151−161.

[50] B. Johnson, N.R.K. Chand, B.K. Sudhakar, G. Srinivasa Rao, Chemical durability, thermal stability and spectroscopic studies of the influence of Ni^{2+} ions in oxyfluorophosphate glasses, J. Mater. Sci. - Mater. Electron. 27 (2016) 8833−8847.

[51] K. Joseph, M. Premila, G. Amarendra, K.V. GovindanKutty, C.S. Sundar, P.R. Vasudeva Rao, Structure of cesium loaded iron phosphate glasses: An infrared and Raman spectroscopy study, J. Nucl. Mater. 420 (2012) 49−53.

[52] Y.M. Lai, X.F. Liang, G.F. Yin, S.Y. Yang, J.X. Wang, H.X. Zhu, H.T. Yu, Infrared spectra of iron phosphate glasses with gadolinium oxide, J. Mol. Struct. 1004 (2011) 188−192.

[53] J. Massera, K. Bourhis, L. Petit, M. Couzi, L. Hupa, M. Hupa, J.J. Videau, T. Cardinal, Effect of the glass composition on the chemical durability of zinc-phosphate-based glasses in aqueous solutions, J. Phys. Chem. Solids 74 (2013) 121−127.